Surface & Coatings Technology 261 (2015) 398–403

Contents lists available at ScienceDirect

Surface & Coatings Technology

journal homepage: www.elsevier.com/locate/surfcoat

Microstructure and properties of (Cr:N)-DLC films deposited by a hybrid beam technique

Wei Yang [a,b], Yongchun Guo [a], Dapeng Xu [a], Jinhua Li [a], Ping Wang [a], Peiling Ke [b], Aiying Wang [b,*]

[a] School of Materials Science and Chemical Engineering, Xi'an Technological University, Xi'an 710032, China
[b] Key Laboratory of Marine New Materials and Related Technology, Zhejiang Key Laboratory of Marine Materials and Protection Technology, Ningbo Institute of Material Technology & Engineering, Chinese Academy of Sciences, Ningbo 315201, PR China

ARTICLE INFO

Article history:
Received 25 June 2014
Accepted in revised form 21 October 2014
Available online 25 October 2014

Keywords:
316L stainless steel
(Cr:N)-DLC film
Microstructure
Wear

ABSTRACT

In this paper, diamond-like carbon (DLC) films doped with CrN nano-crystalline were prepared on 316L stainless steel using a hybrid beam deposition system (including a linear ion source (LIS) and a DC magnetron sputtering of Cr target). The microstructure and composition of the films were studied using transmission electron microscopy (TEM), X-ray photoelectron spectroscopy (XPS) and Raman spectroscopy. Mechanical and tribological properties were investigated using nano-indentation and tribological tester. The results showed that an N doping could significantly influence the microstructure and properties of the as-deposited films. On one hand, the N atoms doped in the film tended to form Cr–N, –C═N–H and C–N bonding, which would enhance the binding strength. On the other hand, the formation of CrN/CrC nano-crystalline due to N doping dispersed in the amorphous DLC matrix could play an important role and increase its hardness. In addition, the (Cr:N)-DLC showed low friction coefficient and wear rate compared with the Cr-DLC film.

1. Introduction

Diamond-like carbon (DLC) films have been extensively studied for more than two decades due to the excellent properties [1–3]. Owing to the high level of internal stresses, DLC films have a tendency to show weak adhesion, thereby limiting their deposition thickness and field of applications [4,5]. The incorporation of other elements (like Cr, Ti or Si) into the DLC films provides an effective way to improve their properties [6–10]. Numerous research reports show that the formation of the carbide phase in the DLC film is useful to improve the mechanical property, but the wear behavior was deteriorated [11]. Pal et al. studied the incorporation of N into the Cr-DLC by a hybrid plasma-assisted CVD/PVD process and found that this microstructure could enhance the film performance, such as higher hardness and lower intrinsic stresses, but it showed the higher coefficient of friction and wear rate [12]. Our previous works have proved that Ti and N co-doping into DLC ((Ti:N)-DLC) films formed by a hybrid beam deposition system could improve their wear and corrosion resistance [13], which provided an effective way to overcome the disadvantage of this (Cr:N)-DLC film.

In this paper, Cr and N will be co-doped into DLC films using a hybrid beam deposition system to form the (Cr:N)-DLC film for improving the performances of 316L stainless steel substrate due to its special microstructure [14–16]. Different from the literature [12], nitrogen could be fully ionized by the ion source to increase its content in the (Cr:N)-DLC film and promote the formation of CrN in the DLC matrix. So the designed (Cr:N)-DLC film using a hybrid beam deposition system in this experiment might be expected to have high contents of Cr and N to form CrN in the DLC matrix. Subsequently, the microstructure, mechanical properties and wear behavior of the Cr-DLC and (Cr:N)-DLC films were comparatively investigated. It is expected that the designing microstructure of DLC film with CrN crystalline has the potential to enhance the film performance [17].

2. Experimental details

Silicon (100) wafers and 316L stainless steel were used as the substrates, which were cleaned ultrasonically in acetone and ethanol, and dried in air before being put into the vacuum chamber. The Cr-DLC and (Cr:N)-DLC films were deposited on the substrates by a hybrid ion beam deposition system consisting of a DC magnetron sputtering with a 120 mm (W) × 380 mm (L) rectangular Cr target (99.99%) and a 380 mm (L) linear anode-layer ion sources (LIS), as shown in the literature [18]. Prior to deposition, the substrates were sputter-cleaned for 5 min using Ar ion with a bias voltage of −100 V. The base pressure was evacuated to a vacuum of 2.9×10^{-3} Pa. During the Cr-DLC film deposition process, hydrocarbon gas (C_2H_2, 15 sccm) was introduced into the linear ion source to obtain the hydrocarbon ions for DLC deposition. The Ar sputtering gas with 60 sccm was supplied to the magnetron sputter for Cr sputtering with a sputtering current of 2.5 A. To obtain the (Cr:N)-DLC film, hydrocarbon (C_2H_2) and N_2 (C_2H_2/N_2 ratio 10 sccm:5 sccm) were introduced into the linear ion source and the

* Corresponding author.
E-mail addresses: yangwei_smx@163.com (W. Yang), aywang@nimte.ac.cn (A. Wang).

http://dx.doi.org/10.1016/j.surfcoat.2014.10.044
0257-8972/

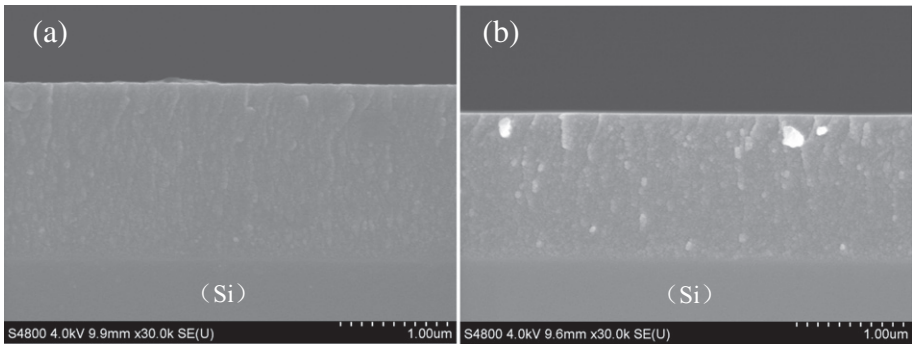

Fig. 1. Cross-section SEM images of (a) Cr-DLC film and (b) (Cr:N)-DLC film.

Ar sputtering gas with 60 sccm was supplied to the magnetron sputter for Cr doping. Typical values of LIS voltage and current were 1138 ± 20 V and 0.15 A, respectively. The DC power supplied to the sputtering gun was about 1100 W (440 V, 2.5 A). During the Cr-DLC and (Cr:N)-DLC films deposition process, the work pressure was all at 4.8×10^{-1} Pa. A negative pulsed bias voltage of −100 V was applied to the substrate. The deposition time was 1 h, and the deposition rates of Cr-DLC and (Cr:N)-DLC films were 20.8 nm/min and 16.7 nm/min, respectively.

High-resolution transmission electron microscopy of the films was performed on Tecnai F20 electron microscope operated at 200 keV with a point-to-point resolution of 0.24 nm. The TEM specimens were prepared by peeling off the films from the NaCl crystalline substrates, which were dissolved in deionized water. The composition and chemical state of Cr, C and N in the Cr-DLC and (Cr:N)-DLC films on the Si substrate were investigated by X-ray photoelectron spectroscopy (XPS). The binding energies were referenced to the C1s line at 285.0 eV. Raman spectroscopy with an incident Ar^+ beam at a wavelength of 514.5 nm was used to measure the atomic bonds of films on the 316L stainless steel substrate. Microhardness measurements were conducted using the nano-indentation technique in a continuous stiffness measurement (CSM) mode with a maximum indentation depth of 500 nm. The characteristic hardness of the films on the 316 stainless steel substrate was chosen in the depth of 200 nm of the film thickness. The adhesion of the films on the 316 stainless steel substrate was assessed by a scratch tester performed on a Rockwell diamond indenter with a conical tip of 0.2 mm in radius. The normal load of the indenter was linearly ramped from the minimum (1 N) to the maximum (120 N) during scratching. In the test, the scratch length was 3.00 mm and the scratch speed was 5 mm/min. The loads corresponding to the films peeled to the substrates were used to evaluate the binding strength. Each binding experiment of the coated sample was repeated 3 times. The tribological behaviors of the films on the 316 stainless steel substrate were measured on a rotary ball-on-disk tribometer at room temperature with a relative humidity of 60–70% under the sliding conditions. A steel ball (SUJ-2, HRC60) with a diameter of 6 mm was used as the friction counter body. All the tests were performed at 0.1 m/s sliding velocity for a distance of 500 m and the applied load was 3 N.

3. Results and discussion

3.1. Coating characteristics

Fig. 1 shows the cross-sectional SEM images of the Cr-DLC and (Cr:N)-DLC films deposited on Si substrates. The film thickness obtained from the cross-section images decreased from 1248 nm for the Cr-DLC film to 1002 nm for the (Cr:N)-DLC film, implying that the Cr and N co-doping decreased the growth rate of the films deposited by the hybrid beams. Obviously, the two films were all composed of the small and compact spherical particles, and for the (Cr:N)-DLC film, the size of these particles increased and the segregated bigger "bright" structure was observed. Compared with the Cr-DLC film, the changes of thickness and microstructure of (Cr:N)-DLC film might be due to a different reaction occurring for the N doping into the film, which resulted in different components of the film.

Fig. 2 illustrates the typical TEM images and corresponding diffraction pattern of the (Cr:N)-DLC film with 27.5 at.% Cr and 6.63 at.% N. Fig. 2(a) shows a microstructure with the uniform nano-scale particle-like embedded into the amorphous carbon matrix. A self-organized multilayered structure of bright and dark bands is clearly observed in the films. The distinct rings displayed in the diffraction patterns (Fig. 2(b)) are identified to be the (111), (200), (220), (311) and (222) reflections of the face-centered (fcc) CrN or CrC crystal. Lattice fringes are observed indicating that defective nanoparticles with crystal structure are existing in the (Cr:N)-DLC film. It is noted that the difference of lattice spacing of the (111), (200), (220) (311) and (222) planes of CrN and CrC is too small to be distinguished by the electron diffraction. So the granular nanocomposite structure of the (Cr:N)-DLC film could be composed of the (111), (200), (220), (311) and (222) planes of CrC and/or CrN. Wei Dai has been reported that the plan-view TEM images and corresponding sectional area electron diffraction (SAED) patterns of the Cr-DLC film, using similar process conditions,

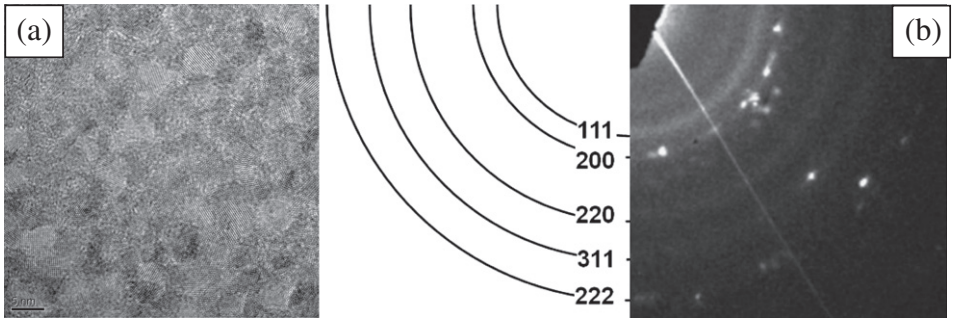

Fig. 2. Typical TEM micrograph and corresponding diffraction pattern of (Cr:N)-DLC film.

show sharp crystalline diffraction rings identified to be the (111), (200), (220) and (311) reflections of the face-centered (FCC) chromium carbide structure [19]. So the microstructure of the (Cr:N)-DLC film is different from the Cr-DLC film, which has been further analyzed by XPS.

The bonding natures of samples were investigated using XPS analysis. Fig. 3(a) presents XPS spectra of Cr-DLC film showing mainly Cr and C peaks. Elemental analysis showed that the Cr-DLC has 77.8 at.% C and 20.8 at.% Cr. Since a very small O peak (about 1.4 at.%) was present, indicating that little Cr oxide was formed in the film. Fig. 3(b) presents XPS spectra of (Cr:N)-DLC film showing mainly Cr, N and C peaks. The (Cr:N)-DLC has 64.4 at.% C, 27.5 at.% Cr and 6.6 at.% N, and also a very small O peak (about 1.5 at.%) was observed. Fig. 3(c) and (d) showed the C1s high-resolution XPS spectra from the Cr-DLC and (Cr:N)-DLC films, giving three peaks at 283.0, 284.8 and 286.7 eV, which are assigned to Cr–C, C–C (C–H) and C–O bonds, respectively [20–22]. It has been reported that the C1s binding energy of graphite (sp^2) and the diamond (sp^3) was 284.3 eV and 284.8 eV [9], respectively. So the C–C (C–H) bond in

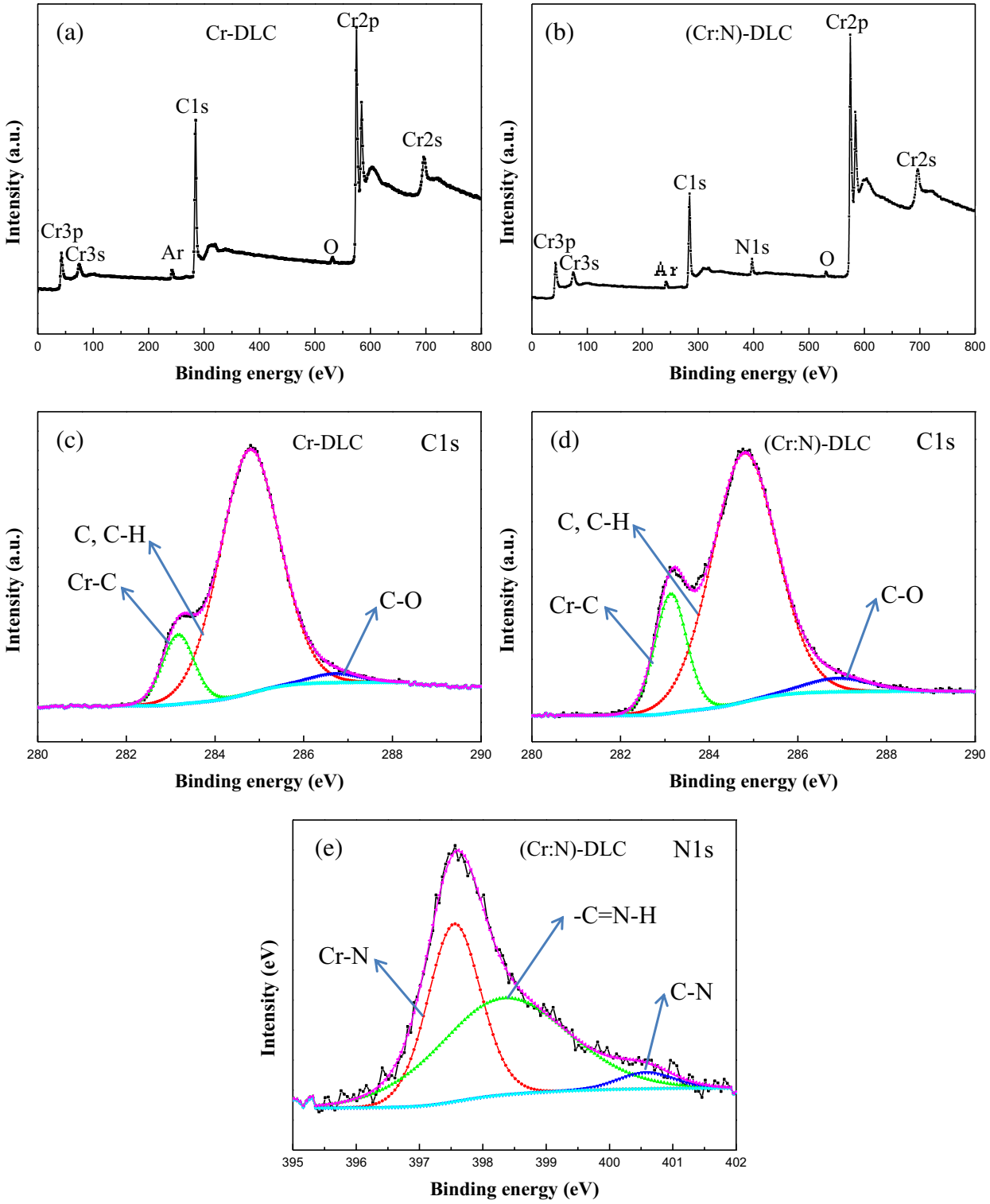

Fig. 3. XPS spectra, typical N1s and C1s high-resolution XPS spectra of Cr-DLC film and (Cr:N)-DLC film.

Fig. 3(c) and (d) can be further deconvoluted into two peaks around 284.3 eV and 284.8 eV, which is assigned to sp^2 (C–H) and sp^3 (C–H) bonded carbon atoms. Subsequently, the sp^2/sp^3 ratio is measured by taking the ratio of the sp^2 peak area over the sp^3 peak area. The sp^2/sp^3 ratio is 4.00 for the Cr-DLC and 6.97 for (Cr:N)-DLC, which implies an increase in sp^2 content. In addition, it was noted that the content of Cr–C bond in the (Cr:N)-DLC film was higher than that in the Cr-DLC film. Fig. 3(e) shows the N1s high-resolution XPS spectra from the (Cr:N)-DLC film. The corresponding N1s peak was fitted into Cr–C, –C═N–H and C–N bonds [23]. In view of the TEM and XPS results, the nitride crystal in the (Cr:N)-DLC film has been formed compared with the Cr-DLC film. It is known that N_2 can be fully ionized by the ion source in this experiment, as a result, the ionized N is incorporated in the C network of DLC forming –C═N–H and Cr–N bonds. It has been reported that this microstructure of the designed (Cr:N)-DLC films was very useful to increase the properties of the coated samples [12,13].

The atomic bond structure of DLC films can be characterized by the intensity ratio, the full width at half maximum (FWHM) values or the position of each peak of their Raman spectra between 900 and 1800 cm^{-1} [24]. The Raman spectra were recorded on both Cr-DLC and (Cr:N)-DLC films on the Si substrates, as shown in Fig. 4. All the peaks are deconvoluted after the Gaussian fitting method. The relative ratio of the D peak to G peak (I_D/I_G) and the position of G peak can be used to characterize the sp^3/sp^2 bonding ratio. In particular, the bonding ratio of sp^3/sp^2 is the most dominant factor assessing the quality of DLC films [25]. Details of Raman spectra for the two coated specimens are listed in Table 1. It can be seen that the position of the G peak and the integrated I_D/I_G ratio of the (Cr:N)-DLC film are found to be higher than that of the Cr-DLC film. This implies that the (Cr:N)-DLC film tends to have a lower ratio of sp^3/sp^2. This result is consistent with the XPS analysis.

Table 1
Details of Raman spectra for the two coated specimens.

Film	D peak, cm^{-1}	G peak, cm^{-1}	I_D/I_G	$FWHM_D/FWHM_G$
Cr-DLC	1365	1543	1.61	2.14
(Cr:N)-DLC	1368	1545	2.14	2.10

It is known that adhesion of DLC films on 316L stainless steel substrates, as a predominant characteristic in tribological uses, is generally weak [26,27]. In order to improve adhesion of coatings on various materials, numerous doping metals (e.g. Ti, Cr, W, and Cu) have been usually used. Also N doping into DLC film is beneficial to decrease the residual stress and improve the binding strength [28]. In this work, the critical load of the (Cr:N)-DLC coated sample has a higher critical load (84.5 N) than that of the Cr-DLC coated one (73.8 N). This may be related to a decreased stress relaxation caused by N incorporation in the network and/or formation of CrC and/or CrN nanoparticles in this (Cr:N)-DLC film.

3.2. Mechanical properties

The hardness-depth curve obtained from nanoindentation test is given in Fig. 5, which shows that the hardness of the two films gradually increased with the indentation depth. When the penetration depth is at the range from 0 nm to 200 nm, the hardness values of the Cr-DLC and (Cr:N)-DLC films increase sharply to a maximum with the penetration depth increasing, which is approximately 12.8 GPa and 15.5 GP at a displacement of about 200 nm, respectively. The hardness values of the two films are much higher than that of the 316 stainless steel substrate (2.8 GPa). Furthermore, it has been obtained that the surface roughness Ra of this substrate was 3.33 nm. So the abrupt increase of the hardness values at the initial stage may be due to some factors including surface roughness and elastic deformation from both tip and the sample surface. It is noted that the hardness of the (Cr:N)-DLC film is higher than that of Cr-DLC film, which may be due to the formation –C═N–H and Cr–N bonds in the (Cr:N)-DLC film. The hardness of the film is related to sp^3/sp^2 bonding ratio and the amount of hydrogen [29]. The above XPS and Raman analysis show that the ratio of sp^3/sp^2 in (Cr:N)-DLC decreases, but the formation of –C═N–H and C–N may be beneficial in keeping high hardness of (Cr:N)-DLC film. Moreover, the hydrogen is

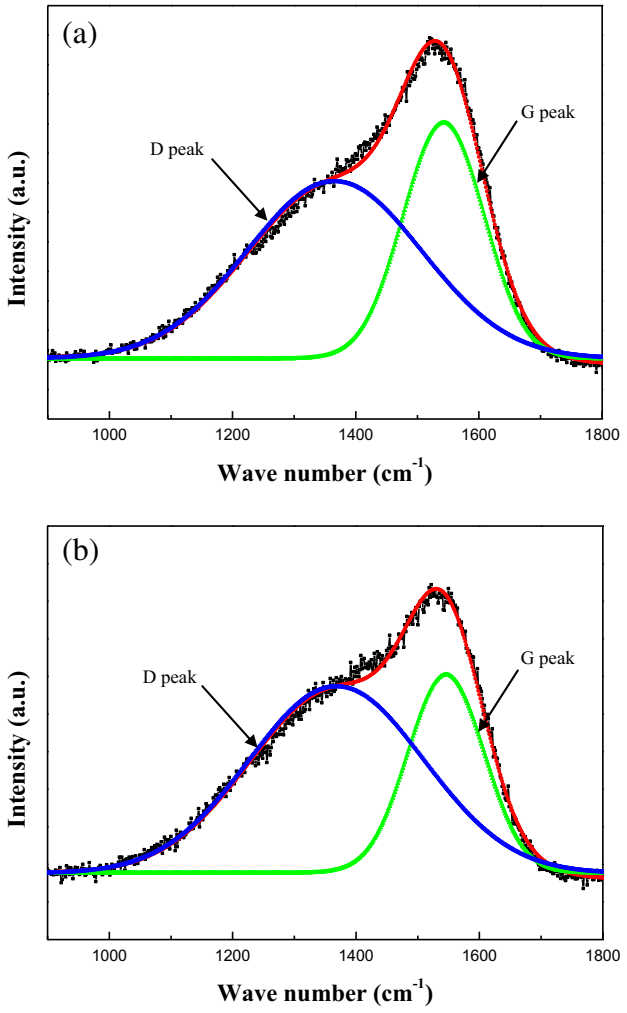

Fig. 4. Raman spectra of (a) Cr-DLC film and (b) (Cr:N)-DLC film.

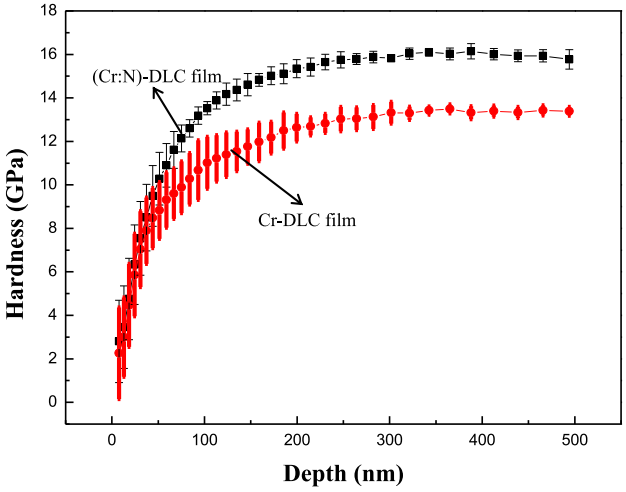

Fig. 5. Hardness versus displacement of Cr-DLC film and (Cr:N)-DLC film.

believed to play a crucial role in the bonding configuration of carbon atoms for stabilizing sp^3 bonding of carbon species. These results are in good agreement with the values reported in the literature [29].

3.3. Tribological properties

Fig. 6 shows the friction coefficient evolution of the Cr-DLC and (Cr:N)-DLC coated specimens at a normal load of 3 N. It can be found that friction for the two coated specimens initially exhibits a sharp drop in friction coefficient due to transfer layer formation [30]. The (Cr:N)-DLC coated specimen presents a low and fluctuating friction coefficient of about 0.16. Furthermore, the friction coefficient even slightly increases with sliding distance. The reasons of increased friction coefficient could be attributed to the fact that hard phases and nanocomposite structure were formed in the (Cr:N)-DLC film, which could be seen from Fig. 2. For the Cr-DLC coated specimen, it shows a high friction coefficient of about 0.23 and performs a non-stable friction behavior with continuous oscillatory peaks during the friction process. As a result, the (Cr:N)-DLC coated specimen exhibits a low wear rate (1.7×10^{-7} mm^3/Nm) compared with the Cr-DLC coated specimen (4.9×10^{-7} mm^3/Nm). Fig. 7 reveals the cross-section profiles of the Cr-DLC and (Cr:N)-DLC films after friction test. Compared to the (Cr:N)-DLC film, as shown in Fig. 7(b), the Cr-DLC film shows a deep and broad wear track (Fig. 7(a)). According to these above results, it can be concluded that the wear resistance of (Cr:N)-DLC film on 316L stainless steel was greatly improved under the friction condition. It is noted that, contrary to the results in reference [12], in this work the friction coefficient of the (Cr:N)-DLC coated sample is lower than that of the sample Cr-DLC. From the XPS analysis in this experiment, it is obtained that the (Cr:N)-DLC film has much higher Cr and N contents compared with that in reference [12]. Also the deposited (Cr:N)-DLC film shows a low sp^3/sp^2 ratio compared with the Cr-DLC. It is known that the hard carbide phase can improve the hardness and the low sp^3/sp^2 ratio results in the graphitization in the transfer layer [31,32]. Furthermore, the formation of more nitride incorporated in the C network will change the microstructure of DLC film and improve the binding strength between the film and the substrate. So the difference of C, Cr and N contents of the (Cr:N)-DLC film due to the experimental conditions resulted in the different microstructure, and then it showed a different tribological result from the reference.

It is known that the durability of the DLC films in the friction process was significantly different due to their different microstructure [7,10]. The friction and wear behaviors of the DLC films mainly correlate with their composition and microstructure. Dai et al. [19] have previously reported that the Cr-doped DLC film with chromium carbide phase,

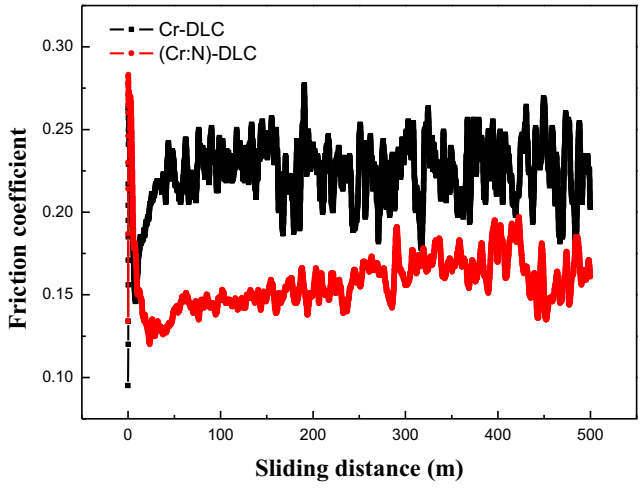

Fig. 6. Coefficient of friction (COF) of the films on 316L stainless steel as a function of sliding distance.

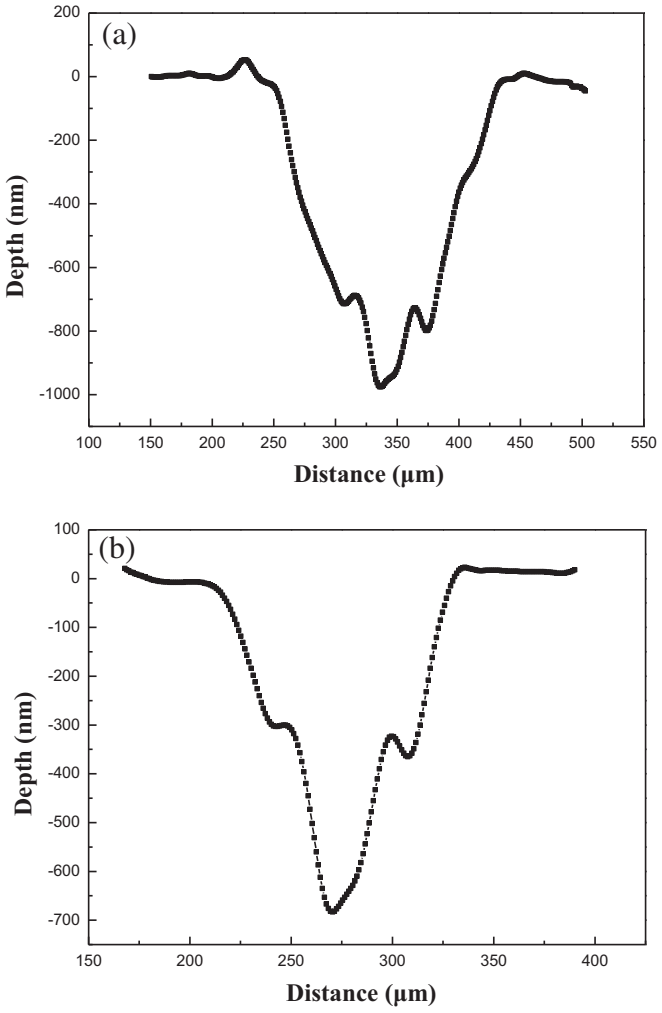

Fig. 7. Cross-section profiles of the wear tracks of (a) Cr-DLC film and (b) (Cr:N)-DLC film.

causing abrasive wear, had a higher friction coefficient compared to that of the non-doped DLC film. In our experiment, it has been obtained that the (Cr:N)-DLC film improves the wear resistance of 316L stainless steel compared with the Cr-DLC film. The difference between the two films is that the CrN and/or CrC nanoparticles of (Cr:N)-DLC film are formed and cause the improved mechanical property, binding strength and thermal stability [17]. Furthermore, it is obtained that the ratio of sp^3/sp^2 in the (Cr:N)-DLC film has been decreased, which may result in the graphitized layer formed easily during the friction process. As a result, the friction coefficient and the wear rate of this designed nanocomposite film remain at a low level compared with the Cr-DLC film.

4. Conclusions

The Cr-DLC and (Cr:N)-DLC films deposited by the hybrid beams system were characterized for their structure and properties. The (Cr:N)-DLC film showed a small and compact spherical particle structure. In the (Cr:N)-DLC film, CrC and/or CrN crystalline phases were obtained. The ionized N was incorporated in the C network (–C═N–H and C–N) while the remaining N combined with Cr to partly transform into Cr–N. Compared to Cr-DLC, the (Cr:N)-DLC film with a low ratio of sp^3/sp^2 was found to increase the binding strength and hardness. These effects may be attributed to the formation of nanometersized CrC and/or CrN crystalline phase in this film. The (Cr:N)-DLC film also showed low friction coefficient and wear rate. This behavior is

attributed to its special microstructure, increased binding strength and high hardness.

Acknowledgments

The authors gratefully acknowledge the financial support of the Natural Science Foundation of China (Grant No. 51201176), National Basic Research Program of China (2012CB619602-4) and Shaanxi Provincial Education Department Program (2013JK0678).

References

[1] J. Choi, S. Nakao, J. Kim, M. Ikeyama, T. Kato, Diamond Relat. Mater. 16 (2007) 1361–1364.
[2] H. Mohrbacher, J.P. Celis, Diamond Relat. Mater. 4 (1995) 1267–1270.
[3] H.A. Castillo, E. Restrepo-Parra, P.J. Arango-Arango, Appl. Surf. Sci. 257 (2011) 2665–2668.
[4] A.Y. Wang, H.S. Ahn, K.R. Lee, J.P. Ahn, Appl. Phys. Lett. 86 (2005) 111902–111904.
[5] A.Y. Wang, K.R. Lee, J.P. Ahn, J.H. Han, Carbon 44 (2006) 1826–1832.
[6] C.W. Zou, H.J. Wang, L. Feng, S.W. Xue, Appl. Surf. Sci. 286 (2013) 137–141.
[7] G.J. Ma, S.L. Gong, G.Q. Lin, L. Zhang, G. Sun, Appl. Surf. Sci. 258 (2012) 3045–3050.
[8] D. Hofmann, S. Kunkel, K. Bewilogua, R. Wittorf, Surf. Coat. Technol. 215 (2013) 357–363.
[9] F. Zhao, H.X. Li, Li Ji, Y.J. Wang, H.D. Zhou, J.M. Chen, Diamond Relat. Mater. 19 (2010) 342–349.
[10] M. Lubwama, K.A. McDonnell, J.B. Kirabira, A. Sebbit, K. Sayers, D. Dowling, B. Corcoran, Surf. Coat. Technol. 206 (2012) 4585–4593.
[11] W. Dai, P.L. Ke, A.Y. Wang, Vacuum 85 (2011) 792–797.
[12] S.K. Pal, J.C. Jiang, E.I. Meletis, Surf. Coat. Technol. 201 (2007) 7917–7923.
[13] W. Yang, P.L. Ke, Y. Fang, H. Zheng, A.Y. Wang, Appl. Surf. Sci. 270 (2013) 519–525.
[14] M. Schlögl, B. Mayer, J. Paulitsch, P.H. Mayrhofer, Thin Solid Films 545 (2013) 375–379.
[15] P.Z. Shi, J. Wang, C.X. Tian, Z.G. Li, G.D. Zhang, D.J. Fu, B. Yang, Surf. Coat. Technol. 228 (2013) S534–S537.
[16] J.L. Lin, W.D. Sproul, J.J. Moore, Mater. Lett. 89 (2012) 55–58.
[17] H.K. Li, G.Q. Lin, C. Dong, Chin. J. Inorg. Chem. 25 (2010) 517–521.
[18] W. Dai, G.S. Wu, A.Y. Wang, J. Mater. Eng. 1 (2009) 44–47.
[19] W. Dai, G.S. Wu, A.Y. Wang, Diamond Relat. Mater. 19 (2010) 1307–1315.
[20] V. Singh, J.C. Jiang, E.I. Meletis, Thin Solid Films 489 (2005) 150–158.
[21] D. Bourgoin, S. Turgeon, G.G. Ross, Thin Solid Films 357 (1999) 246–253.
[22] G.M. Wilson, S.O. Saied, S.K. Field, Thin Solid Films 515 (2007) 7820–7828.
[23] Data base http://www.lasurface.com/database/elementxps.php.
[24] W.G. Cui, Q.B. Lai, L. Zhang, F.M. Wang, Surf. Coat. Technol. 205 (2010) 1995–1999.
[25] J. Robertson, Mater. Sci. Eng. R 37 (2002) 129–281.
[26] M.M. Morshed, B.P. McNamara, D.C. Cameron, M.S.J. Hashmi, Surf. Coat. Technol. 163–164 (2003) 541–545.
[27] B. Podgornik, J. Vizintin, Diamond Relat. Mater. 10 (2001) 2232–2237.
[28] K.H. Lee, R. Ohta, H. Sugimura, Y. Inoue, O. Takai, H. Sugimura, Thin Solid Films 475 (2005) 308–312.
[29] A. Tibrewala, E. Peiner, R. Bandorf, S. Biehl, H. Lüthje, J. Micromech. Microeng. 17 (2007) S77–S82.
[30] W.J. Hsieh, C.C. Lin, U.S. Chen, Y.S. Chang, H.C. Shih, Diamond Relat. Mater. 14 (2005) 93–97.
[31] Y. Liu, E.I. Meletis, J. Mater. Sci. 32 (1997) 3491–3495.
[32] L.F. Xia, G. Li, Wear 264 (2008) 1077–1084.